

# Continuous-Time Control Synthesis for Multiple Quadrotors under Signal Temporal Logic Specifications

Yating Yuan

**Abstract**—Ensuring continuous-time control of multiple quadrotors in constrained environments under signal temporal logic (STL) specifications is challenging due to nonlinear dynamics, safety constraints, and disturbances. This letter proposes a two-stage framework to address this challenge. First, exponentially decaying tracking error bounds are derived with multidimensional geometric control gains obtained via differential evolution. These bounds are less conservative, while the resulting tracking errors exhibit smaller oscillations and improved transient performance. Second, leveraging the time-varying bounds, a mixed-integer convex programming (MICP) formulation generates piecewise Bézier reference trajectories that satisfy STL and velocity limits, while ensuring inter-agent safety through convex-hull properties. Simulation results demonstrate that the proposed approach enables formally verifiable multi-agent coordination in constrained environments, with provable tracking guarantees under bounded disturbances.

**Index Terms**—Signal temporal logic planning, multiple quadrotors, geometric control

## I. INTRODUCTION

As drone technology progresses, quadrotors are increasingly required to execute complex tasks in confined environments—particularly narrow passages and strict terminal zones [1]. In this context, signal temporal logic (STL) offers a formal language to define tasks over continuous signals with explicit time semantics. However, ensuring STL satisfaction for multi-agent systems under nonlinear dynamics and disturbances remains challenging [2].

Therefore, various approaches have been explored to ensure STL satisfaction for multi-agent systems. Recently, Model Predictive Control (MPC) has been widely adopted due to its efficiency and outstanding capacity for addressing complex constraints and uncertainty [3]–[7]. [3] employs an MPC-based controller under continuous-time STL with stricter specifications, using smooth robustness to improve efficiency in multi-agent tasks, though this relaxation may compromise soundness. [4]–[7] apply Distributed MPC (DMPC) to cooperative control in multi-agent systems by solving local problems with neighbor communication, offering a balance between scalability and coordination. While effective for multi-agent efficiency, these methods generally lack guarantees for continuous-time STL satisfaction. To address this challenge, [7] assumes piecewise constant inputs and derives Lipschitz bounds on robustness functions to guarantee continuous-time satisfaction. However, DMPC typically operates in discrete time and remains limited by iterative computation.

Yating Yuan is with the Department of Applied Mathematics, University of Waterloo, 200 University Avenue, Waterloo, ON, Canada N2L 3G1. (email: yating.yuan@uwaterloo.ca)

In contrast, closed-loop strategies such as Control Barrier Functions (CBFs) and Prescribed Performance Control (PPC) directly enforce continuous-time STL satisfaction via real-time state-feedback control. [8] proposes decentralized time-varying CBFs with switching logic but lacks fixed-time guarantees. [9] introduces fixed-time CBFs (TFCBFs) with least-violation optimization to handle task conflicts. [10] employs higher-order CBFs with feedback linearization for temporal waypoint tracking. PPC provides predefined performance guarantees [11] and has been extended to multi-agent STL control. [12] addresses formation and sequencing tasks, [13] focuses on leader-follower coordination, and [14] introduces contract-based decomposition for distributed implementation. While these methods offer robustness and operate in continuous time, they remain limited to specific specification classes, require careful parameter tuning, and may suffer from input discontinuities under switching.

Other Lyapunov-based feedback controllers for nonlinear systems [15], [16] have been combined with MILP-based STL planning to ensure continuous-time satisfaction [17], but tend to be conservative in narrow environments due to fixed tracking error bounds [16]. Euclidean-space controllers may suffer from singularities or inconsistent position–attitude coordination when applied to quadrotors. To address these issues, this letter employs geometric control [18]–[23] as a nonlinear feedback strategy on  $SE(3)$ , enabling agile maneuvers and direct handling of quadrotor dynamics.

**Contributions:** The two main contributions include: 1) a differential evolution-based method that computes geometric control gains for position and attitude tracking, yielding time-varying error bounds with exponential decay that are less conservative than those in [23], and producing tracking errors with smaller oscillations as validated in experiments; 2) an MICP-based STL planning method that constructs  $C^4$ -continuous Bézier curves that satisfy continuous-time STL and velocity constraints while ensuring inter-agent safety via the convex-hull property.

The rest of the letter is organized as follows. Section II introduces the basic concepts, including the dynamical model, geometric control, Bézier curves, and signal temporal logic. Section III formulates the control synthesis problem under STL specifications. Section IV presents the analysis of error bounds, sufficient conditions, and the differential evolution-based optimization. Section V formulates the MICP-based optimization problem for generating desired trajectories for multiple quadrotors. Experimental and simulation results are provided in Section VI.

## II. PRELIMINARIES

**Notation:** Let  $\mathbb{Y} \subset \mathbb{R}^d$ , where  $d = 3$  is assumed in this letter. Moreover, let  $1_d \in \mathbb{R}^d$  denote the all-ones vector, and  $I_d, 0_{d \times d} \in \mathbb{R}^{d \times d}$  the identity and zero matrices, respectively. The set  $\mathbb{S}_{++}^n$  denotes symmetric positive-definite matrices of size  $n \times n$ . For any  $a \in \mathbb{R}^d$ ,  $|a|$  denotes the element-wise absolute value, and  $\|a\|$  is the Euclidean norm. The maximum and minimum eigenvalues of a matrix  $A$  are denoted by  $\bar{\lambda}(A)$  and  $\underline{\lambda}(A)$ , and  $\text{tr}(A)$  denotes its trace. Let  $T > 0$  define the time horizon, and  $\mathbb{T} = [0, T]$ . For a signal  $y : \mathbb{T} \rightarrow \mathbb{Y}$ , define  $(y, [t_i, t_j]) := \{y(t) \mid t \in [t_i, t_j]\}$ , and let  $(y, t) := (y, [t, T])$ . Define a convex polytope  $\text{Poly}(H, b) := \{x \in \mathbb{R}^d \mid Hx \leq b\}$ , with  $H \in \mathbb{R}^{r \times d}$  and  $b \in \mathbb{R}^r$ . Let  $H_i$  and  $b_i$  denote the  $i$ -th row of  $H$  and entry of  $b$ , respectively. The number of rows in  $H$  is denoted  $\text{Row}(H)$ .

### A. Quadrotor Dynamics Model

In this work, the reference frames used for quadrotor dynamics are depicted in Fig. 1. An inertial reference frame  $\mathcal{I} = \{e_1, e_2, e_3\}$  is defined such that  $e_3$  points upward, opposite to gravity. A body-fixed frame  $\mathcal{B} = \{b_1, b_2, b_3\}$  is attached at the quadrotor's center of mass, with  $b_1$  pointing forward,  $b_2$  pointing laterally, and  $b_3$  pointing upward along the rotor thrust.

The configuration space of the quadrotor is the special Euclidean group  $\text{SE}(3)$ , parameterized by a rotation matrix  $R \in \text{SO}(3)$  and position  $p \in \mathbb{R}^3$  [24, Chapter 3]. The Lie algebra  $\mathfrak{so}(3)$  of  $\text{SO}(3)$  is the space of skew-symmetric matrices. The hat map  $\hat{\cdot} : \mathbb{R}^3 \rightarrow \mathfrak{so}(3)$  is defined as:

$$\hat{\omega} = \begin{pmatrix} 0 & -\omega_3 & \omega_2 \\ \omega_3 & 0 & -\omega_1 \\ -\omega_2 & \omega_1 & 0 \end{pmatrix}, \quad \omega = \begin{bmatrix} \omega_1 \\ \omega_2 \\ \omega_3 \end{bmatrix} \in \mathbb{R}^3, \quad (1)$$

satisfying  $\hat{u}v = u \times v$  for  $u, v \in \mathbb{R}^3$ . Its inverse, the vee map  $\vee : \mathfrak{so}(3) \rightarrow \mathbb{R}^3$ , recovers the vector  $\omega$  from  $\hat{\omega}$ .

Table I lists physical variables of the quadrotor dynamics model, which follow the model in [19] as:

$$\dot{p}(t) = v(t), \quad (2)$$

$$\dot{v}(t) = -ge_3 + m^{-1}f(t)R(t)e_3, \quad (3)$$

$$\dot{R}(t) = R(t)\hat{\omega}(t), \quad (4)$$

$$\hat{\omega}(t) = J^{-1}(-\omega(t) \times J\omega(t) + \tau(t)), \quad (5)$$

### B. Geometric Control

Let  $y_d : \mathbb{T} \rightarrow \mathbb{Y}$  be a desired  $\mathcal{C}^4$  position trajectory<sup>1</sup>. As presented in Fig. 1, the desired rotation matrix  $R_d(t) = [b_{d,1}(t), b_{d,2}(t), b_{d,3}(t)] \in \text{SO}(3)$  where  $b_{d,1}(t)$ ,  $b_{d,2}(t)$  and  $b_{d,3}(t)$  are chosen as follows [19], [23]. The details are also illustrated in Appendix II. The corresponding angular velocity is  $\omega_d(t) = (R_d^\top(t)\dot{R}_d(t))^\vee \in \mathbb{R}^3$ .

Let  $y_{tr} : \mathbb{T} \rightarrow \mathbb{R}^3$  be a tracking trajectory with rotation matrix  $R(t) \in \text{SO}(3)$  and angular velocity  $\omega(t) \in \mathbb{R}^3$ . The positive gain matrices  $K_p$ ,  $K_v$ ,  $K_R$ , and  $K_\omega$  are defined as

<sup>1</sup>A function is  $\mathcal{C}^k$  if it is  $k$ -times continuously differentiable. Computing  $\dot{\omega}_d(t)$  requires the fourth derivative of  $y_d$  with respect to time.

TABLE I: Common variables in quadrotor dynamics.

| Symbol                       | Physical meaning  |
|------------------------------|---|
| $m \in \mathbb{R}$           | The total mass  |
| $g \in \mathbb{R}$           | The gravitational acceleration, $g = 9.81 \text{ m/s}^2$      |
| $J \in \mathbb{S}_{++}^3$    | The inertia matrix  |
| $p(t) \in \mathbb{R}^3$      | The position of the center of mass                            |
| $v(t) \in \mathbb{R}^3$      | The velocity  |
| $R(t) \in \text{SO}(3)$      | The rotation matrix, $b_i(t) = R(t)e_i$ , $i \in \{1, 2, 3\}$ |
| $\omega(t) \in \mathbb{R}^3$ | The angular velocity in the body-fixed frame                  |
| $f_i(t) \in \mathbb{R}$      | The thrust of the $i$ -th propeller along $b_3$               |
| $f(t) \in \mathbb{R}$        | The total thrust $f(t) = \sum_{i=1}^4 f_i(t)$                 |
| $\tau(t) \in \mathbb{R}^3$   | The torque  |

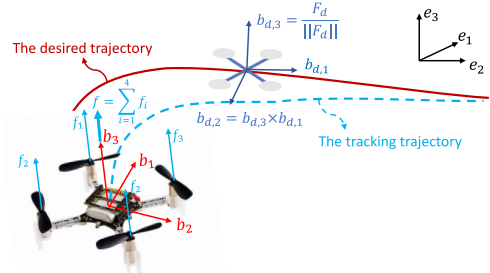


Fig. 1: The inertial frame  $\mathcal{I}$ , the body frame  $\mathcal{B}$ , and desired body axes  $b_{d,1}(t)$ ,  $b_{d,2}(t)$ ,  $b_{d,3}(t)$  representing the desired orientation  $R_d(t)$ .

$K_* = \text{diag}(k_{*1}, k_{*2}, k_{*3})$ , for  $* \in \{p, v, R, \omega\}$ . Define the position, velocity, weighted rotational, and angular velocity errors as  $e_p(t)$ ,  $e_v(t)$ ,  $e_{K,R}(t)$ ,  $e_\omega(t) \in \mathbb{R}^3$ , and the attitude error function  $\Psi_K(t) \in \mathbb{R}$  [21]:

$$e_p(t) := y_{tr}(t) - y_d(t), \quad (6)$$

$$e_v(t) := \dot{y}_{tr}(t) - \dot{y}_d(t), \quad (7)$$

$$e_{K,R}(t) := \frac{1}{2} (K_R R_d^\top(t) R(t) - R^\top(t) R_d(t) K_R)^\vee, \quad (8)$$

$$e_\omega(t) := \omega(t) - R^\top(t) R_d(t) \omega_d(t), \quad (9)$$

$$\Psi_K(t) := \frac{1}{2} \text{tr} (K_R (I_3 - R_d^\top(t) R(t))). \quad (10)$$

In this letter, the force  $f(t)$  and torque  $\tau(t)$  are defined as:

$$f(t) = F_d^\top(t) R(t) e_3, \quad (11)$$

$$F_d(t) = -K_p e_p(t) - K_v e_v(t) + mge_3 + m\ddot{y}_d(t), \quad (12)$$

$$\tau(t) = -e_{K,R}(t) - K_\omega e_\omega(t) + \omega(t) \times J\omega(t) - J(\hat{\omega}(t) R^\top(t) R_d(t) \omega_d(t) - R^\top(t) R_d(t) \dot{\omega}_d(t)). \quad (13)$$

*Proposition 1 (Adapted from [20]; see also [21, Prop. 1]):* Supposing  $K_R$  has distinct positive diagonal entries, define

$$h_1 = \min \{k_{R_1} + k_{R_2}, k_{R_1} + k_{R_3}, k_{R_2} + k_{R_3}\},$$

$$h_2 = \max \left\{ (k_{R_1} - k_{R_2})^2, (k_{R_1} - k_{R_3})^2, (k_{R_2} - k_{R_3})^2 \right\},$$

$$h_3 = \max \{k_{R_1} + k_{R_2}, k_{R_1} + k_{R_3}, k_{R_2} + k_{R_3}\}.$$

If  $\Psi_K(t) < \psi < h_1$  for some positive  $\psi$ , then

$$g_1 \|e_{K,R}(t)\|^2 \leq \Psi_K(t) \leq g_2 \|e_{K,R}(t)\|^2, \quad (14)$$

where  $g_1 = \frac{h_1}{h_2+h_3^2}$  and  $g_2 = \frac{h_3}{h_1(h_1-\psi)}$ .

### C. Bézier Curves

In this letter, a continuous-time desired position trajectory  $y_d(t) : \mathbb{T} \rightarrow \mathbb{Y}$  is parameterized by  $N$  piecewise Bézier curves. Specifically, with a sampling time  $\Delta t = \frac{T}{N}$ , the desired trajectory  $y$  is defined as follows:

$$y_d(t) = \begin{cases} B_0(t), & t \in [t_0, t_1], \\ B_1(t), & t \in [t_1, t_2], \\ \vdots \\ B_{N-1}(t), & t \in [t_{N-1}, t_N], \end{cases} \quad (15)$$

where  $t_k = k\Delta t$  for  $k = \{0, 1, \dots, N-1\}$ . Each  $B_k(t)$  is an  $n$ -degree Bézier curve defined as

$$B_k(t) = \sum_{i=0}^n b_i^n(\tau) c_{k,i}, \quad \tau = \frac{t - t_k}{\Delta t} \in [0, 1], \quad (16)$$

where  $c_{k,i}$  is the  $i$ -th control point of the  $k$ -th Bézier curve, and  $b_i^n(\tau) = \binom{n}{i}(1-\tau)^{n-i}\tau^i$  is the  $n$ -degree Bernstein polynomial. Since  $\sum_{i=0}^n b_i^n(\tau) = 1$  for any  $\tau \in [0, 1]$ , this implies that each  $B_k(t)$  lies within the convex hull  $\mathcal{CH}_k := \text{conv}\{c_{k,0}, \dots, c_{k,n}\}$ .

### D. Signal Temporal Logic

Given a vector-valued function  $\mu$  defined on  $\mathbb{Y}$ , an atomic predicate  $\pi$  can be constructed as  $\pi := \mu(x) = b - Hx \geq 0$ , which evaluates to *true* iff the point  $x$  lies inside the convex polytope  $\text{Poly}(H, b)$ . In this work, only predicates of this form are considered. In particular,  $x \in \text{Poly}(H, b)$  if and only if  $\mu(x) \geq 0$ . The syntax of STL is defined as:

$$\varphi := \pi \mid \neg\varphi \mid \varphi_1 \wedge \varphi_2 \mid \varphi_1 \vee \varphi_2 \mid \varphi_1 \mathcal{U}_I \varphi_2, \quad (17)$$

where  $\neg$ ,  $\wedge$  and  $\vee$  are negation, conjunction and disjunction operators, respectively;  $I = [a, b] \subseteq \mathbb{T}$  is a bounded time interval and  $I$  is a non-singleton bounded interval ( $a < b$ ); and  $\mathcal{U}_I$  is *Until*, which means  $\varphi_2$  will be true at some point within  $I$ , *until* that moment, and  $\varphi_1$  has to remain true. Other temporal operators, *Eventually* ( $\diamond$ ) and *Always* ( $\square$ ) can be formulated by the above operators. For instance,  $\diamond_I \varphi := \text{True } \mathcal{U}_I \varphi$  and  $\square_I \varphi := \neg(\diamond_I \neg\varphi)$ .

**Definition 1:** (STL semantics [25]) Given an STL specification  $\varphi$  and a continuous-time signal  $y : \mathbb{T} \rightarrow \mathbb{Y}$ , STL semantics is defined over suffixes of signals as follows:

$$\begin{aligned} (y, t) \models \pi & \Leftrightarrow \mu(y(t)) > 0; \\ (y, t) \models \neg\varphi & \Leftrightarrow \neg((y, t) \models \varphi); \\ (y, t) \models \varphi_1 \wedge \varphi_2 & \Leftrightarrow (y, t) \models \varphi_1 \wedge (y, t) \models \varphi_2; \\ (y, t) \models \varphi_1 \vee \varphi_2 & \Leftrightarrow (y, t) \models \varphi_1 \vee (y, t) \models \varphi_2; \\ (y, t) \models \diamond_I \varphi & \Leftrightarrow \exists t' \in \tilde{I}, (y, t') \models \varphi; \\ (y, t) \models \square_I \varphi & \Leftrightarrow \forall t' \in \tilde{I}, (y, t') \models \varphi; \\ (y, t) \models \varphi_1 \mathcal{U}_{[a,b]} \varphi_2 & \Leftrightarrow \exists t' \in \tilde{I} (y, t') \models \varphi_2 \\ & \wedge \forall t'' \in [t, t'], (y, t'') \models \varphi_1, \end{aligned}$$

where  $\tilde{I} = (t+I) \cap \mathbb{T}$  and  $t+I = [t+a, t+b]$ . The notation  $(y, t) \models \varphi$  indicates that the signal suffix  $(y, t)$  satisfies the STL formula  $\varphi$ , while  $(y, t) \not\models \varphi$  denotes that it does not. For brevity, note that  $y \models \varphi$  if  $(y, 0) \models \varphi$ .

A time-varying robust trajectory is introduced to characterize whether a trajectory robustly satisfies the STL specification  $\varphi$  at each time instant.

**Definition 2:** (Time-varying robust trajectory [26]) Given a function  $\rho^\varphi : \mathbb{T} \rightarrow \mathbb{R}_{>0}$ , a position trajectory  $y : \mathbb{T} \rightarrow \mathbb{Y}$  is said to be  $\rho^\varphi$ -robust with respect to an STL specification  $\varphi$  if  $\tilde{y} \models \varphi$  for every trajectory  $\tilde{y}$  satisfying

$$\|\tilde{y}(t) - y(t)\| \leq \rho^\varphi(t), \quad \forall t \in \mathbb{T}. \quad (18)$$

Note that  $\rho^{\ell, \varphi}(t)$  is denoted as the time-varying robustness margin associated with the  $\ell$ -th agent's desired trajectory with respect to the STL specification  $\varphi$ .

## III. PROBLEM STATEMENT

Given an STL specification  $\varphi$ , this letter aims to synthesize desired trajectories and a feedback controller for multiple quadrotors, ensuring their tracked trajectories  $y_{tr}$  satisfy  $\varphi$ . To formalize the required robustness margin, a lower time-varying robustness bound  $\gamma(t)$  is introduced as follows.

**Definition 3:** (Lower time-varying robustness bound) Let  $\gamma_c > 0$  be a constant safety margin and let  $\Gamma : \mathbb{T} \rightarrow \mathbb{R}_{>0}$  be a non-increasing function, i.e.,  $\Gamma(t) \leq \Gamma(0)$  for all  $t \in \mathbb{T}$ . The lower time-varying robustness bound  $\gamma(t)$  is defined as

$$\gamma(t) := \Gamma(t) + \gamma_c, \quad t \in \mathbb{T}. \quad (19)$$

Here  $\Gamma(t)$  bounds the position tracking error, and  $\gamma_c$  serves as a physical safety margin (e.g., quadrotor size). Thus, if  $y_d(t) \models \varphi$  with robustness margin  $\rho^\varphi(t)$  and  $\rho^\varphi(t) \geq \gamma(t) > \Gamma(t)$ , implying

$$\|y_{tr}(t) - y_d(t)\| \leq \Gamma(t) < \rho^\varphi(t) \Rightarrow y_{tr}(t) \models \varphi. \quad (20)$$

Hence, the synthesis problem splits into two subproblems.

**Problem 1:** Compute the multidimensional control gains for the geometric controller in (11)–(13) and determine the position error bound, thereby obtaining a non-increasing lower time-varying robustness bound  $\Gamma(t)$ .

**Problem 2:** Given an STL specification  $\varphi$ , a reference trajectory  $y_d^\ell$  in (15) for each  $\ell$ -th agent is generated, such that  $y_d^\ell \models \varphi$  with a robustness margin  $\rho^{\ell, \varphi}(t) \geq \gamma(t) \geq \Gamma(t)$ , while ensuring multi-agent safety and satisfying the element-wise velocity constraints  $|\dot{y}_d^\ell(t)| \leq v_{\max}$  and  $|\dot{y}_{tr}^\ell(t)| \leq v_{\max}$ .

## IV. TRACKING ERROR BOUNDS

In this section, the error bounds of the geometric controller and the corresponding initial conditions are first analyzed in Section IV-A. Then, an optimization problem is formulated in Section IV-B to determine control gains such that the resulting error bounds satisfy the requirements stated in *Problem 1* in Section III.

### A. Time-varying Error Bounds Analysis

The following analysis relies on known properties of geometric control [21]–[23] and the controller defined in (6)–(13). To obtain tractable bounds on the tracking errors, a physical limit on the desired acceleration is first imposed.

**Assumption 1** ([22]): Assume there exists a positive vector  $b_a \in \mathbb{R}_{>0}^3$  such that the second derivative of  $y_d$  satisfies

$$|mge_3 + m\ddot{y}_d(t)| \leq b_a, \quad \forall t \in \mathbb{T} \quad (21)$$

This assumption bounds the desired trajectory's acceleration and facilitates subsequent analysis of error bounds.

1) *Lyapunov Function for Translation-error Dynamics:*

Let the translation-error vector be  $z_1^\top(t) := [e_p^\top(t) \ e_v^\top(t)]$ . Choose the Lyapunov candidate  $\mathcal{V}_1$  as

$$\mathcal{V}_1(t) := z_1^\top(t) M_1 z_1(t), \quad (22)$$

where

$$M_1 = \frac{1}{2} \begin{bmatrix} K_p & c_1 I_3 \\ c_1 I_3 & m I_3 \end{bmatrix} \in \mathbb{S}_{++}^6, \quad (23)$$

$$c_1 = \nu_1 \min \left\{ \sqrt{m \lambda(K_p)}, \min_{i=1,2,3} \left( \frac{4mk_{p_i} k_{v_i}}{k_{v_i}^2 + 4mk_{p_i}} \right) \right\}, \quad (24)$$

with a tuning constant  $\nu_1 \in (0, 1)$ . Its time derivative is

$$\dot{\mathcal{V}}_1(t) = -z_1^\top(t) W_1 z_1(t) - \Delta_f^\top(t) \begin{bmatrix} c_1 \\ m \end{bmatrix} I_3 z_1(t), \quad (25)$$

where

$$W_1 = \frac{1}{2m} \begin{bmatrix} 2c_1 K_p & c_1 K_v \\ c_1 K_v & 2m(K_v - c_1 I_3) \end{bmatrix} \in \mathbb{S}_{++}^6, \quad (26)$$

$$\Delta_f(t) = \|F_d(t)\| \left( (b_{3,d}(t) - b_{3,d}^\top(t) b_3(t)) b_3(t) \right). \quad (27)$$

2) *Lyapunov Function for Rotational-error Dynamics:*

Define  $z_2^\top(t) := [e_{K,R}^\top(t) \ e_\omega^\top(t)]$  as the rotational error vector and let the Lyapunov candidate function be

$$\mathcal{V}_2(t) := \frac{1}{2} e_\omega^\top(t) J e_\omega(t) + \Psi_K(t) + c_2 e_{K,R}^\top(t) e_\omega(t), \quad (28)$$

where

$$c_2 := \nu_2 \min \left\{ \sqrt{2g_m \lambda(J)}, \frac{\sqrt{2\lambda(K_\omega)}}{\text{tr}(K_R)}, \min_{i=1,2,3} \frac{4J_i k_{\omega_i}}{2\sqrt{2} J_i \text{tr}(K_R) + k_{\omega_i}^2} \right\}, \quad (29)$$

with  $g_m = \min\{g_1, g_2\}$  and  $\nu_2 \in (0, 1)$ . From (14),  $\mathcal{V}_2(t)$  is bounded by

$$z_2^\top(t) M_{2,1} z_2(t) \leq \mathcal{V}_2(t) \leq z_2^\top(t) M_{2,2} z_2(t), \quad (30)$$

where  $M_{2,1}, M_{2,2} \in \mathbb{S}_{++}^6$  are defined as

$$M_{2,1} = \frac{1}{2} \begin{bmatrix} 2g_1 I_3 & c_2 I_3 \\ c_2 I_3 & J \end{bmatrix}, M_{2,2} = \frac{1}{2} \begin{bmatrix} 2g_2 I_3 & c_2 I_3 \\ c_2 I_3 & J \end{bmatrix}. \quad (31)$$

The time derivative  $\dot{\mathcal{V}}_2(t)$  satisfies:

$$\dot{\mathcal{V}}_2(t) \leq -z_2^\top(t) W_2 z_2(t), \quad (32)$$

where

$$W_2 = \begin{bmatrix} c_2 J^{-1} & \frac{c_2}{2} K_\omega J^{-1} \\ \frac{c_2}{2} K_\omega J^{-1} & K_\omega - \frac{c_2}{\sqrt{2}} \text{tr}(K_R) I_3 \end{bmatrix} \in \mathbb{S}_{++}^6. \quad (33)$$

3) *Time-varying Lyapunov Function Bound (see Appendix III for details):* Combining (30) and (32) and applying the Rayleigh quotient inequality yields

$$\dot{\mathcal{V}}_2(t) \leq -\lambda \left( M_{2,2}^{-\frac{1}{2}} W_2 M_{2,2}^{-\frac{1}{2}} \right) \mathcal{V}_2(t). \quad (34)$$

Applying the Grönwall–Bellman inequality yields

$$\mathcal{V}_2(t) \leq e^{-\beta t} \mathcal{V}_2(0), \quad (35)$$

where  $\beta := \lambda \left( M_{2,2}^{-\frac{1}{2}} W_2 M_{2,2}^{-\frac{1}{2}} \right)$ . This further implies that  $\sqrt{\mathcal{V}_2(t)} \leq \mathcal{L}_2(\mathcal{V}_2(0), t)$  where

$$\mathcal{L}_2(\mathcal{V}_2(0), t) := e^{-\frac{\beta}{2} t} \sqrt{\mathcal{V}_2(0)}. \quad (36)$$

Likewise, the bound on  $\dot{\mathcal{V}}_1(t)$  in (25) can be obtained as:

$$\dot{\mathcal{V}}_1(t) \leq -(\alpha_0 - \alpha_1 \sqrt{\mathcal{V}_2(t)}) \mathcal{V}_1(t) + \alpha_2 \sqrt{\mathcal{V}_2(t) \mathcal{V}_1(t)}, \quad (37)$$

where

$$\alpha_0 = \underline{\lambda} \left( M_1^{-\frac{1}{2}} W_1 M_1^{-\frac{1}{2}} \right), \quad (38)$$

$$\alpha_1 = \left\| \begin{bmatrix} c_1 \\ m \end{bmatrix} I_3, I_3 \right\| M_1^{-\frac{1}{2}} \left\| [K_p, K_v] M_1^{-\frac{1}{2}} \right\| \beta', \quad (39)$$

$$\alpha_2 = m \|b_a\| \left\| \begin{bmatrix} c_1 \\ m \end{bmatrix} I_3, I_3 \right\| M_1^{-\frac{1}{2}} \beta', \quad (40)$$

$$\beta' = \left\| [I_3, 0_{3 \times 3}] M_{2,1}^{-\frac{1}{2}} \right\| \sqrt{\frac{4g_2}{h_1}}. \quad (41)$$

Since  $\sqrt{\mathcal{V}_2(t)} \leq \mathcal{L}_2(\mathcal{V}_2(0), t)$ , using Grönwall's inequality to (37) yields  $\sqrt{\mathcal{V}_1(t)} \leq \mathcal{L}_1(\mathcal{V}_1(0), \mathcal{V}_2(0), t)$  where

$$\mathcal{L}_1(\mathcal{V}_1(0), \mathcal{V}_2(0), t) = e^{-\frac{\alpha_0 t}{2}} \left[ e^{\frac{\alpha_1 \sqrt{\mathcal{V}_2(0)}}{\beta}} \sqrt{\mathcal{V}_1(0)} + \frac{\alpha_2 \sqrt{\mathcal{V}_2(0)}}{2} \int_0^t e^{\frac{1}{2}(\alpha_0 - \beta)s} ds \right]. \quad (42)$$

It can be seen that both  $\mathcal{L}_1(\mathcal{V}_1(0), \mathcal{V}_2(0), t)$  and  $\mathcal{L}_2(\mathcal{V}_2(0), t)$  provide exponentially decaying upper bounds on the tracking errors over time. If there exist  $\bar{\mathcal{V}}_1 \geq \mathcal{V}_1(0)$  and  $\bar{\mathcal{V}}_2 \geq \mathcal{V}_2(0)$ , then,  $\mathcal{L}_1(\bar{\mathcal{V}}_1, \bar{\mathcal{V}}_2, t) \geq \mathcal{L}_1(\mathcal{V}_1(0), \mathcal{V}_2(0), t)$  holds. From (22), there exist the time-varying tracking error bounds  $\|e_p(t)\| \leq \mathcal{L}_p(t)$  and  $\|e_v(t)\| \leq \mathcal{L}_v(t)$  where

$$\mathcal{L}_p(t) := \left\| [I_3, 0_{3 \times 3}] M_1^{-\frac{1}{2}} \right\| \mathcal{L}_1(\bar{\mathcal{V}}_1, \bar{\mathcal{V}}_2, t), \quad (43)$$

$$\mathcal{L}_v(t) := \left\| [0_{3 \times 3}, I_3] M_1^{-\frac{1}{2}} \right\| \mathcal{L}_1(\bar{\mathcal{V}}_1, \bar{\mathcal{V}}_2, t). \quad (44)$$

Compared to [23], the proposed bounds are tighter, as they avoid over-approximating the entire system and are derived directly from  $\mathcal{L}_1(\bar{\mathcal{V}}_1, \bar{\mathcal{V}}_2, t)$ . The following initial conditions specify how to choose  $\bar{\mathcal{V}}_1$  and  $\bar{\mathcal{V}}_2$  to determine the bounds  $\mathcal{L}_p(t)$  and  $\mathcal{L}_v(t)$ .

*Proposition 2 (Initial conditions):* Given a  $\mathcal{C}^4$ -continuous trajectory  $y_d : \mathbb{T} \rightarrow \mathbb{R}^3$  that satisfies (21), if the tracking trajectory  $y_{tr}$  meets the following initial error conditions:

$$\Psi(0) \leq \alpha_\psi \psi, \quad (45)$$

$$\frac{1}{2} e_\omega^\top(0) J e_\omega(0) \leq (1 - \alpha_\psi) \psi, \quad (46)$$

$$\mathcal{V}_1(0) \leq \bar{\mathcal{V}}_1, \quad (47)$$

where  $\alpha_\psi \in (0, 1)$ ,  $\psi \in (0, h_1)$ , and  $\bar{\mathcal{V}}_1 \in (0, \infty)$  are user-defined. There exists

$$\bar{\mathcal{V}}_2 = \left( 1 + c_2 \sqrt{\frac{2(1 - \alpha_\psi)}{\lambda(J)g_1}} \right) \psi \geq \mathcal{V}_2(0), \quad (48)$$

such that (43) and (44) are valid.

The detailed proof can be found on [Appendix IV](#).

### B. Optimization-based Control Gains

Selecting appropriate control gains is challenging due to the system's nonlinear dynamics. This letter obtains the control gains by minimizing  $\mathcal{L}(\mathcal{V}_1, \mathcal{V}_2, t)$  to reduce the error bounds. To set up the optimization concisely, let  $\zeta = \frac{\alpha_0 - \beta}{2}$ ,  $\bar{x} = \bar{\mathcal{V}}_1$ , and  $\bar{y} = \bar{\mathcal{V}}_2$ .  $\dot{\mathcal{L}}_1(\bar{x}, \bar{y}, t)$  is monotonic when  $\zeta \neq 0$  and affine when  $\zeta = 0$ , thus having at most one root. Let  $t_c$  be the unique solution to  $\frac{d}{dt} \mathcal{L}(\bar{x}, \bar{y}, t) = 0$ . Since  $\ddot{\mathcal{L}}_1(\bar{x}, \bar{y}, t_c) < 0$ , it follows that

$$\mathcal{L}_{1, \max}(\bar{x}, \bar{y}) = \max_{t \in \mathbb{T}} \mathcal{L}_1(\bar{x}, \bar{y}, t) = \mathcal{L}_1(\bar{x}, \bar{y}, t^*), \quad (49)$$

where  $t^* := \max(0, \min(t_c, T)) \in \mathbb{T}$  with

$$t_c = \begin{cases} \frac{2(\alpha_2 \sqrt{\bar{y}} - \alpha_0 \sqrt{\bar{x}} e^{\frac{\alpha_1 \sqrt{\bar{y}}}{\beta}})}{\alpha_0 \alpha_2 \sqrt{\bar{y}}}, & \text{if } \zeta = 0, \\ \frac{1}{\zeta} \ln \left( \frac{\alpha_0 (\alpha_2 \sqrt{\bar{y}} - (\alpha_0 - \beta) \sqrt{\bar{x}} e^{\frac{\alpha_1 \sqrt{\bar{y}}}{\beta}})}{\beta \alpha_2 \sqrt{\bar{y}}} \right), & \text{if } \zeta \neq 0. \end{cases} \quad (50)$$

Furthermore, to satisfy the condition in Proposition 1, it is required that  $\Delta_{K_R} \geq 3$  where

$$\Delta_{K_R} = \sum_{1 \leq i < j \leq 3} \Delta_{ij}, \Delta_{ij} = \begin{cases} 1, & |K_{R_i} - K_{R_j}| \geq \epsilon_R, \\ 0, & \text{otherwise.} \end{cases} \quad (51)$$

Then, Problem 1 is formulated and solved using the Differential Evolution algorithm, a global optimizer that requires no initial guess and supports parallel computation.

*Problem 1:* The control gains  $\{K_p, K_v, K_R, K_\omega\}$  and auxiliary parameters  $\{\nu_1, \nu_2\}$  are determined by solving the following optimization problem:

$$\begin{aligned} & \arg \min_{\substack{K_p, K_v, K_R, K_\omega, \\ \nu_1, \nu_2}} \mathcal{L}_{1, \max}(\bar{\mathcal{V}}_1, \bar{\mathcal{V}}_2) \\ & \text{such that } 0 < \nu_1, \nu_2 < 1, \\ & \Delta_{K_R} \geq 3 \quad (\text{Proposition 1}), \\ & \underline{k} \leq K_{p_i}, K_{v_i}, K_{R_i}, K_{\omega_i} \leq \bar{k}, \quad i \in \{1, 2, 3\}. \end{aligned} \quad (52)$$

Here,  $\underline{k}$  and  $\bar{k}$  denote the lower and upper bounds of the control gains, respectively.

## V. REFERENCE TRAJECTORY CONSTRUCTION

This section formulates an optimization problem over the control points of Bézier curves to ensure that the desired trajectory satisfies the STL specifications with a robustness margin, thereby guaranteeing that the tracking trajectory also adheres to the same specifications.

After solving Problem 1, the tracking bound  $\mathcal{L}_p(\bar{\mathcal{V}}_1, \bar{\mathcal{V}}_2, t)$  can be obtained. Ensuring both reference trajectories and the

track trajectories satisfy the STL specifications and according to the Definition 3, choose  $\Gamma(t)$  as

$$\Gamma(t) = \begin{cases} \mathcal{L}_p(t^*), & \text{if } t \leq t^*, \\ \mathcal{L}_p(t), & \text{otherwise.} \end{cases} \quad (53)$$

Thus,  $\gamma(t) = \Gamma(t) + \gamma_c$ . All quadrotors are assumed to share the same physical configuration and Lyapunov parameters. If different models are used, it suffices to adapt  $\Gamma(t)$  for each model to account for the corresponding bounds.

*Problem 2:* Given an STL specification  $\varphi$  and  $L$  quadrotors, the objective is to determine each position trajectory  $y_d^\ell : \mathbb{T} \rightarrow \mathbb{R}^3$  ( $1 \leq \ell \leq L$ ), parameterized by  $N$  piecewise  $n$ -degree Bézier curves as defined in (15), where Bézier curve  $B_k^\ell$  is  $\rho^{\ell, \varphi}$ -robustness, with the robustness measure  $\rho^{\ell, \varphi}(t) = \rho_k^{\ell, \varphi}(\mathcal{C}_k^\ell, a_k^\ell) \geq \gamma(t_k) > 0$  for all  $t \in [t_k, t_{k+1}]$  and  $k \in \{0, \dots, N-1\}$ . Here,  $\rho_k^{\ell, \varphi}(\mathcal{C}_k^\ell, a_k^\ell)$  represents the robustness measure of  $B_k^\ell$ , which depends on the maximum acceleration  $a_k^\ell \in \mathbb{R}^d$  and the control points of  $B_k^\ell$ , denoted by  $\mathcal{C}_k^\ell := \{c_{k,i}^\ell\}_{i=0}^n$ . The resulting optimization problem is formulated as a mixed-integer convex program (MICP) to maximize time-varying robustness while minimizing control effort of the reference trajectory.

$$\begin{aligned} & \arg \min_{\mathcal{C}_k^\ell, v_k^\ell, a_k^\ell} \sum_{l=0}^L \sum_{k=0}^{N-1} -\mathcal{W} \rho_k^{\ell, \varphi}(\mathcal{C}_k^\ell, a_k^\ell) + \mathcal{Q} \|v_k^\ell\|_1 + \mathcal{R} \|a_k^\ell\|_1 \\ & \text{such that } B_k^\ell \text{ and } B_{k+1}^\ell \text{ are } \mathcal{C}^4\text{-continuous,} \\ & |(B_k^\ell)'| \leq v_{max}, \\ & (B_k^\ell)'' \text{ satisfies (21)} \\ & \rho_k^{\ell, \varphi}(\mathcal{C}_k^\ell, a_k^\ell) \geq \gamma(t_k), \end{aligned} \quad (54)$$

where  $\mathcal{W}, \mathcal{Q}, \mathcal{R} \in \mathbb{R}$  are user-defined weights,  $v_k^\ell, a_k^\ell \in \mathbb{R}^3$  are the maximum velocity and acceleration of  $B_k$  over  $t \in [t_k, t_{k+1}]$ , respectively.

### A. Dynamic Constraints

The Bézier curves are required to satisfy the dynamic constraints, which apply uniformly to all agents. The index  $\ell$  is omitted in this subsection. A key property is utilized: the  $q$ -th derivative of a degree- $n$  Bézier curve is a degree- $(n-q)$  Bézier curve.

1)  $\mathcal{C}^4$  Continuity Constraints: To ensure  $\mathcal{C}^4$  continuity at the junction  $t = t_{k+1}$  between consecutive Bézier segments  $B_k$  and  $B_{k+1}$ , five constraints are imposed on their control points, expressed as follows for  $q \in \{0, 1, 2, 3, 4\}$ :

$$\sum_{p=0}^q (-1)^p \binom{q}{p} c_{k, n-p} = \sum_{p=0}^q (-1)^{q-p} \binom{q}{p} c_{k+1, p}. \quad (55)$$

These constraints enforce equality of the backward finite differences of the  $k$ -th Bézier curve's end control points and the forward finite differences of the  $(k+1)$ -th Bézier curve's start control points at the junction time.

2) *Velocity Constraints*: Since the Bernstein polynomial of  $B_k$  satisfies  $\sum_{i=0}^{n-1} b_i^{n-1}(\tau) = 1$  for all  $\tau \in [0, 1]$ , then,

$$|\dot{y}_d(t)| \leq \frac{n}{\Delta t} \left| \sum_{i=0}^{n-1} b_i^{n-1}(\tau) \right| \max_i |c_{k,i+1} - c_{k,i}| \leq v_k, \quad (56)$$

where  $v_k$  is the maximum velocity of  $k$ -th Bézier curve. For ensuring  $|\dot{y}_{tr}| \leq v_{\max}$ , choose  $\tilde{\mathcal{L}}_v(t) = \mathcal{L}_v(t^*)$  for  $t \leq t^*$  and  $\tilde{\mathcal{L}}_v(t) = \mathcal{L}_v(t)$  otherwise; then enforce

$$|c_{k,i+1} - c_{k,i}| \leq \frac{v_k \Delta t}{n}, \forall i \in \{0, \dots, n-1\}, \quad (57)$$

$$0 < v_k \leq v_{\max} - \tilde{\mathcal{L}}_v(t_k) \mathbf{1}_3. \quad (58)$$

3) *Acceleration Constraints*: Similarly, to guarantee that  $B_k''$  satisfies (21), let  $\Delta^2 c_{k,i} := c_{k,i+2} - 2c_{k,i+1} + c_{k,i}$ , the acceleration constraints are enforced as

$$|\Delta^2 c_{k,i}| \leq \frac{a_k \Delta t^2}{n(n-1)}, \quad (59)$$

$$\left| g e_3 + \frac{n(n-1)}{\Delta t^2} (\Delta^2 c_{k,i})^\top e_3 \right| \leq b_a, \quad (60)$$

where  $a_k$  is the maximum acceleration of  $k$ -th Bézier curve.

## B. Multi-agent STL Satisfaction Encoding

This section presents an encoding of the STL specification  $\varphi$  to ensure that each agent's Bézier curve and its tracking trajectory  $y_{tr}$  satisfy  $\varphi$ . A binary variable  $z_k^{\ell, \varphi}$  is introduced to indicate whether the Bézier segment  $B_k$  satisfies the specification; specifically, if  $z_k^{\varphi}$  is true, then  $(B_k, t) \models \varphi$  for all  $t \in [t_k, t_{k+1}]$ .

1) *Continuous-time Robustness of Bézier curves*: To ensure that the tracking trajectory satisfies the STL specification, the robustness of the Bézier curves is required to exceed the tracking error bounds.

As stated in *Problem 2*, the robustness of  $B_k^\ell$  is set as  $\rho_k^\varphi(\mathcal{C}_k^\ell, a_k^\ell) = r_k^\ell - \epsilon_k^\ell \geq \gamma(t_k)$ , where  $r_k^\ell \in \mathbb{R}_{>0}$  specifies a positive margin to guarantee that the endpoints of the curve lie strictly within the required set, and  $\epsilon_k \in \mathbb{R}_{>0}$  represents the margin used to constrain the intermediate control points within the same set, subject to acceleration constraints [26].

- Predicate  $\pi$  :

$$z_k^{\ell, \pi} = \bigwedge_{i=1}^{\text{Row}(H)} \left( \bigwedge_{j=\{0, n\}} \frac{b_i - H_i c_{k,j}^\ell}{\|H_i\|_2} \geq r_k^\ell \right) \wedge z_{\epsilon_k^\ell}. \quad (61)$$

- Negation  $\neg \pi$  :

$$z_k^{\ell, \neg \pi} = \bigvee_{i=1}^{\text{Row}(H)} \left( \bigwedge_{j=\{0, n\}} \frac{H_i c_{k,j}^\ell - b_i}{\|H_i\|_2} \geq r_k^\ell \right) \wedge z_{\epsilon_k^\ell}. \quad (62)$$

where

$$z_{\epsilon_k^\ell} := \left( \bigwedge_{j=\{1, n\}} |c_{k,j}^\ell - c_{k,j-1}^\ell| \leq \frac{a_k^\ell \Delta t^2}{2n} \right) \wedge \left( \bigwedge_{j=0}^d \frac{8\epsilon_k^\ell}{3\sqrt{d}\Delta t^2} - |a_{k,j}| \geq 0 \right). \quad (63)$$

Based on the atomic predicates, the logic and temporal operators are constructed as follows. Given the finite interval  $\tilde{I} = (t + I) \cap \mathbb{T}$ , let  $k_\ell = k + \lfloor a/\Delta t \rfloor$  and  $k_r = \min(k + 1 + \lfloor b/\Delta t \rfloor, N - 1)$  for brevity. Assume  $k_\ell < k_r$ , which is a mild assumption since  $a < b$  and  $N - 1$  are the maximum segment index.

- Conjunctions  $\varphi_1 \wedge \varphi_2 : z_k^{\ell, \varphi_1 \wedge \varphi_2} = z_k^{\ell, \varphi_1} \wedge z_k^{\ell, \varphi_2}$ . (64)

- Disjunctions  $\varphi_1 \vee \varphi_2 : z_k^{\ell, \varphi_1 \vee \varphi_2} = z_k^{\ell, \varphi_1} \vee z_k^{\ell, \varphi_2}$ . (65)

- Always  $\square_I \varphi : z_k^{\ell, \square_I \varphi} = \bigwedge_{k'=k_\ell}^{k_r} z_{k'}^{\ell, \varphi}$ . (66)

- Eventually  $\diamond_I \varphi : z_k^{\ell, \diamond_I \varphi} = \bigvee_{k'=k_\ell}^{k_r} z_{k'}^{\ell, \varphi}$ . (67)

- Until  $\varphi = \varphi_1 \mathcal{U}_I \varphi_2 :$

$$z_k^{\ell, \varphi} = \bigvee_{k'=k_\ell}^{k_r} \left( z_{k'}^{\ell, \varphi_2} \wedge \bigwedge_{k''=k}^{k'-1} z_{k''}^{\ell, \varphi_1} \right). \quad (68)$$

2) *Multi-agent Collision Avoidance Encoding*: To ensure safety guarantees between any two agents  $i$  and  $j$  (where  $1 \leq i < j \leq L$ ), for any  $t \in [t_k, t_{k+1}]$ , the distance between their Bézier curves  $B_k^i(t)$  and  $B_k^j(t)$  is required to remain at least  $\epsilon_{\text{inter}}$ . For simplicity,  $\mathcal{CH}_k^i$  and  $\epsilon_k^i$  are grouped into the tuple  $A_k^i = (\mathcal{CH}_k^i, \epsilon_k^i)$ . Then, the multi-agent safety specification is defined as follows:

$$z_{\text{inter}} = \bigwedge_{1 \leq i < j \leq L} \text{safe} \left( A_k^i, A_k^j, \epsilon_{\text{inter}} \right), \quad (69)$$

where

$$\begin{aligned} \text{safe} \left( A_k^i, A_k^j, \epsilon_{\text{inter}} \right) &:= \left( \left\| \text{cent} \left( B_k^i \right) - \text{cent} \left( B_k^j \right) \right\|_1 \right. \\ &\geq \left\| c_{k,0}^i - c_{k,n}^j \right\|_1 + \left\| c_{k,0}^j - c_{k,n}^i \right\|_1 \\ &\left. + 2 \left( \epsilon_k^j + \epsilon_k^i \right) + \epsilon_{\text{inter}} \sqrt{d} \right). \end{aligned} \quad (70)$$

and  $\text{cent}(B_k^i) = \frac{1}{n+1} \sum_{l=0}^n c_{k,l}^i$  is the geometric center of the convex hull  $\mathcal{CH}_k^i$ . The distance between the two curves is bounded by:

$$\left\| B_k^i(t) - B_k^j(t) \right\| \geq \epsilon_{\text{inter}}. \quad (71)$$

The proof of the soundness of the multi-agent safety can be seen in [Appendix I](#).

*Remark 1*: The encoding for multi-agent safety is stricter, as it considers the full convex hull of each Bézier curve necessary to ensure inter-agent safety. However, due to acceleration constraints and a moderate number of control points, the conservatism introduced by the convex-hull approximation remains tractable. Moreover, the  $\ell_1$ -norm is used in place of the  $\ell_2$ -norm to enable convex, piecewise-linear formulations suitable for MICP solvers.

## VI. EXPERIMENTS

In this section, the performance of our algorithm is evaluated on several benchmarks. The algorithm is implemented in Python, where differential evolution is performed using SciPy [27], and the MICP problem is solved using Gurobi [28]. All experiments were conducted on an Apple M1 chip with 8 cores and 16 GB of RAM.

### A. Control Gains

In this letter, the parameters of the quadrotors are adopted as follows [19]:  $J = \text{diag}(8.20, 8.45, 13.77) \times 10^{-2} \text{ kg} \cdot \text{m}^2$ ,  $m = 4.34 \text{ kg}$ ,  $v_{\max} = [2, 2, 2]^\top$ ,  $b_a = [1, 1, 11]^\top$ , and  $\gamma_c = 0.1$ . The initial parameters for solving Problem 1 are selected as follows:  $\psi = 0.04$ ,  $\alpha_\psi = 0.4$ ,  $\bar{V}_1 = 0.5$ , with control gain bounds  $\underline{k} = 1$  and  $\bar{k} = 30$ .

The optimized control gains are obtained as follows.

$$K_p = \text{diag}(17.8, 18.1, 17.8), \quad K_v = \text{diag}(12.5, 12.5, 12.5), \\ K_R = \text{diag}(27.9, 29.9, 28.9), \quad K_\omega = \text{diag}(5.5, 6.2, 2.5).$$

The auxiliary parameters  $\nu_1 = 0.75$  and  $\nu_2 = 0.59$ . Then,  $\bar{V}_2 = 0.06$  is derived from (48). At time  $t^* = 0.04 \text{ s}$ , the maximum theoretical tracking bounds are

$$\mathcal{L}_{1,\max} = 0.76, \quad \mathcal{L}_p(t^*) = 0.36 \text{ m}, \quad \mathcal{L}_v(t^*) = 0.73 \text{ m/s}.$$

### B. Single Case

Consider the specification  $\varphi_1 = (\square_{[0,T]} \neg Y) \wedge (\diamond_{[0,T]} B)$  with  $T = 40 \text{ s}$ , where twenty Bézier ( $N = 19$ ) curves are generated with eleven control points ( $n = 10$ ). This specification requires the quadrotor to pass through an increasingly narrow region and eventually reach a compact target area, as shown in Fig. 2. Moreover, Fig. 3(a) shows the desired and twenty tracking velocities that are bounded by  $v_{\max} = [2, 2, 2]^\top$ .

In this letter, the proposed method is compared to the scalar gain method [23]. Under identical initial error conditions, twenty tracking trajectories are generated for each approach. Fig. 3(b) displays ten of the twenty trajectory pairs (randomly selected for clarity); the proposed method's errors decay more rapidly and exhibit smaller oscillations. Moreover, its error bounds  $\mathcal{L}_p(t)$  and  $\mathcal{L}_v(t)$  are less conservative than [23]. Furthermore, the robustness of the desired Bézier curves  $\rho^{\varphi_1}(t) \geq \mathcal{L}_p(t) \geq \|e_p(t)\|$  for all  $t \in \mathbb{T}$ , which means all the tracking trajectories meet the specification  $\varphi_1$ . Moreover, the steady-state errors for  $t \geq 4 \text{ s}$  in Fig. 3(c) demonstrate that the proposed method achieves lower median errors as well as a narrower interquartile range, confirming its accurate and stable tracking performance.

### C. Multi-agent Case

Consider the specification for multiple quadrotors given by  $\varphi_2 = \bigwedge_{\ell=1}^4 \varphi^\ell$ , where  $\varphi^\ell = (\square_{[0,T]} \neg Y) \wedge (\diamond_{[0,T]} \square_{[0,2]} G) \wedge (\diamond_{[0,T]} B_{\ell'})$ , with  $\{(\ell, \ell')\} = \{(1, 3), (2, 4), (3, 1), (4, 2)\}$  and  $T = 36 \text{ s}$ . Sixteen Bézier trajectories ( $N = 15$ ) are generated using eleven control points per curve ( $n = 10$ ). The results are shown in Fig. 4(a).

To evaluate the safety of the designed multi-agent trajectory, four desired trajectories  $y_d^\ell$  and their corresponding tracking trajectories  $y_{tr}^\ell$  are generated. Fig. 4(b) presents a heatmap of the pairwise minimum distances over the time domain  $\mathbb{T}$ , computed between any two trajectories as

$$\text{dist}_{i,j} = \min_{t \in \mathbb{T}} \|y_i(t) - y_j(t)\| \quad (72)$$

Here,  $y_i(t)$  and  $y_j(t)$  denote either a desired  $y_d^\ell(t)$  or a tracking trajectory  $y_{tr}^\ell(t)$ . As expected, diagonal entries and

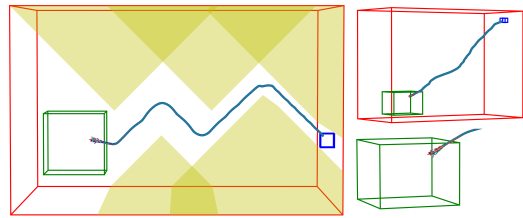


Fig. 2: Trajectory tracking visualization for the single case. The reference trajectory (blue solid line) and twenty tracking trajectories (colored dashed lines) are shown. The left panel shows the top view, while the top-right panel presents the side view, with obstacles omitted for clarity of the trajectories. The bottom-right panel quantifies initial point deviations relative to the reference trajectory.

the distances between each reference trajectory and its corresponding tracking trajectory are both zero (or near zero), indicating perfect or near-perfect tracking performance. All remaining computed minimum distances are greater than  $\epsilon_{\text{inter}} = 0.2 \text{ m}$ , thereby ensuring that the separation between distinct trajectories consistently exceeds the safety threshold.

## VII. CONCLUSION

This letter proposes a continuous-time control framework for multi-quadrotor systems under STL specifications, combining geometric feedback with MICP-based Bézier planning to ensure safety, velocity limits, and STL satisfaction. The method provides provable, time-varying tracking error bounds. While effective, it depends on accurate models and initial error conditions, and incurs significant computational costs for large teams. Future work includes distributed implementations to reduce complexity, extensions to  $SE(3)$  curve planning for full-pose coordination, and integrating learning-based methods for improved adaptability.

## REFERENCES

- [1] Graeme Best, Rohit Garg, John Keller, Geoffrey A Hollinger, and Sebastian Scherer. Multi-robot, multi-sensor exploration of multifarious environments with full mission aerial autonomy. *The International Journal of Robotics Research*, 43(4):485–512, 2024.
- [2] Calin Belta and Sadra Sadraddini. Formal methods for control synthesis: An optimization perspective. *Annual Review of Control, Robotics, and Autonomous Systems*, 2(1):115–140, 2019.
- [3] Yash Vardhan Pant, Houssam Abbas, Rhudii A Quaye, and Rahul Mangharam. Fly-by-logic: Control of multi-drone fleets with temporal logic objectives. In *2018 ACM/IEEE 9th International Conference on Cyber-Physical Systems (ICCP)*, pages 186–197. IEEE, 2018.
- [4] Yuanyuan Zou, Xu Su, Shaoyuan Li, Yugang Niu, and Dewei Li. Event-triggered distributed predictive control for asynchronous coordination of multi-agent systems. *Automatica*, 99:92–98, 2019.
- [5] Xiaoyi Zhou, Yuanyuan Zou, Shaoyuan Li, Xianwei Li, and Hao Fang. Distributed model predictive control for multi-robot systems with conflicting signal temporal logic tasks. *IET Control Theory & Applications*, 16(5):554–572, 2022.
- [6] Ali Tefvik Büyükköçak, Derya Aksaray, and Yasin Yazicioglu. Distributed planning of multi-agent systems with coupled temporal logic specifications. In *AIAA Scitech 2021 Forum*, page 1123, 2021.
- [7] Maria Charitidou and Dimos V Dimarogonas. Distributed MPC with continuous-time STL constraint satisfaction guarantees. *IEEE Control Systems Letters*, 8:211–216, 2024.
- [8] Lars Lindemann and Dimos V Dimarogonas. Decentralized control barrier functions for coupled multi-agent systems under signal temporal logic tasks. In *Proc. of ECC*, pages 89–94. IEEE, 2019.

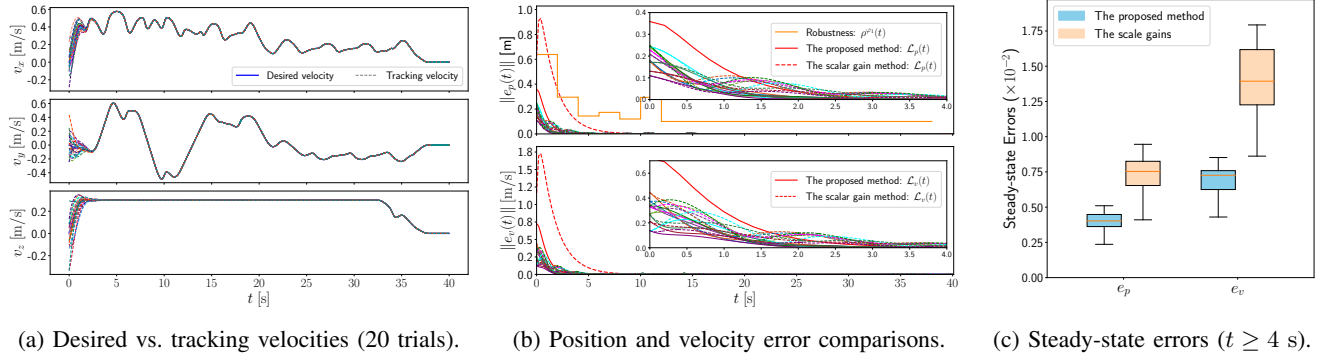


Fig. 3: Velocity tracking performance and error analysis. (a) presents the desired Bézier velocity (solid blue line) and tracking velocities (dashed colored lines), all satisfying  $|v| \leq v_{\max}$ . (b) Tracking errors  $e_p(t)$  and  $e_v(t)$  for the proposed method (solid) and scalar gain method [23] (dashed). Ten of twenty color-matched trajectory pairs with identical initial conditions are shown for clarity. Errors converge after  $t \geq 4$  s. (c) shows that the proposed method attains a lower median error and a narrower interquartile range compared to [23].

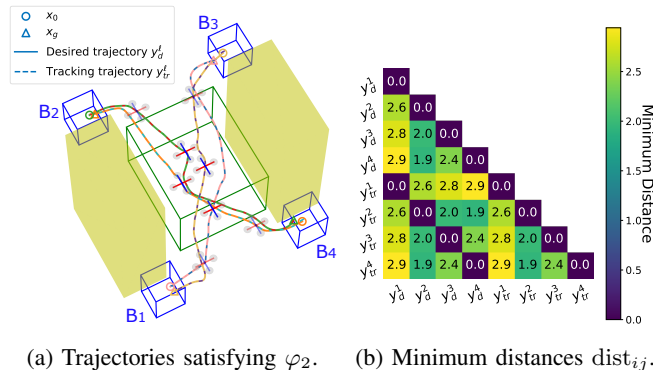


Fig. 4: Multi-agent task results under STL formula  $\varphi_2$ . (a) shows desired (solid) and tracking (dashed) trajectories, along with two sets of quadrotor poses: a faded set at early time  $t = 8.91$  s for visualization, and an opaque set at  $t = 17.42$  s, where the minimum distance 1.9 m occurs in (b). (b) shows that all pairwise distances between agents' trajectories exceed  $\epsilon_{\text{inter}} = 0.2$  m, confirming safety.

[9] Maryam Sharifi and Dimos V Dimarogonas. Fixed-time convergent control barrier functions for coupled multi-agent systems under STL tasks. In *Proc. of ECC*, pages 793–798. IEEE, 2021.

[10] Nishanth Rao, Suresh Sundaram, and Pushpak Jagtap. Temporal waypoint navigation of multi-UAV payload system using barrier functions. In *Proc. of ECC*, pages 1–6. IEEE, 2023.

[11] Xiangwei Bu. Prescribed performance control approaches, applications and challenges: A comprehensive survey. *Asian Journal of Control*, 25(1):241–261, 2023.

[12] Lars Lindemann, Christos K Verginis, and Dimos V Dimarogonas. Prescribed performance control for signal temporal logic specifications. In *Proc. of CDC*, pages 2997–3002. IEEE, 2017.

[13] Fei Chen and Dimos V Dimarogonas. Funnel-based cooperative control of leader-follower multi-agent systems under signal temporal logic specifications. In *Proc. of ECC*, pages 906–911. IEEE, 2022.

[14] Siyuan Liu, Adnane Saoud, and Dimos V Dimarogonas. Controller synthesis of collaborative signal temporal logic tasks for multi-agent systems via assume-guarantee contracts. *IEEE Transactions on Automatic Control*, 2025.

[15] Chuchu Fan, Kristina Miller, and Sayan Mitra. Fast and guaranteed safe controller synthesis for nonlinear vehicle models. In *Computer Aided Verification*, pages 629–652. Cham, 2020. Springer International

Publishing.

[16] Yash Vardhan Pant, He Yin, Murat Arcak, and Sanjit A. Seshia. Co-design of control and planning for multi-rotor UAVs with signal temporal logic specifications. In *Proc. of ACC*, pages 4209–4216, 2021.

[17] Dawei Sun, Jingkai Chen, Sayan Mitra, and Chuchu Fan. Multi-agent motion planning from signal temporal logic specifications. *IEEE Robotics and Automation Letters*, 7(2):3451–3458, 2022.

[18] Weibin Gu, Stefano Primates, and Alessandro Rizzo. Robust adaptive control for aggressive quadrotor maneuvers via  $SO(3)$  and backstepping techniques. *Robotics and Autonomous Systems*, page 104942, 2025.

[19] Taeyoung Lee, Melvin Leok, and N Harris McClamroch. Geometric tracking control of a quadrotor UAV on  $SE(3)$ . In *Proc. of CDC*, pages 5420–5425. IEEE, 2010.

[20] Taeyoung Lee. Robust adaptive attitude tracking on  $SO(3)$  with an application to a quadrotor UAV. *IEEE Transactions on Control Systems Technology*, 21(5):1924–1930, 2012.

[21] Davide Invernizzi and Marco Lovera. Geometric tracking control of a quadcopter tiltrotor UAV. *IFAC-PapersOnLine*, 50(1):11565–11570, 2017.

[22] Kanishke Gamedara, Mahdis Bisheban, Evan Kaufman, and Taeyoung Lee. Geometric controls of a quadrotor UAV with decoupled yaw control. In *Proc. of ACC*, pages 3285–3290. IEEE, 2019.

[23] Mohamed Serry, Haocheng Chang, and Jun Liu. Reach-avoid control synthesis for a quadrotor UAV with formal safety guarantees. *arXiv preprint arXiv:2405.20502*, 2024.

[24] Kevin M. Lynch and Frank C. Park. *Modern Robotics: Mechanics, Planning, and Control*. Cambridge University Press, 2017.

[25] Alexandre Donzé and Oded Maler. Robust satisfaction of temporal logic over real-valued signals. In *Proc. of FORMATS*, 2010.

[26] Yating Yuan, Thanin Quartz, and Jun Liu. Signal temporal logic planning with time-varying robustness. *IEEE Control Systems Letters*, 2024.

[27] Pauli Virtanen, Ralf Gommers, Travis E. Oliphant, Matt Haberland, Tyler Reddy, David Cournapeau, Evgeni Burovski, Pearu Peterson, Warren Weckesser, Jonathan Bright, Stéfan J. van der Walt, Matthew Brett, Joshua Wilson, K. Jarrod Millman, Nikolay Mayorov, Andrew R. J. Nelson, Eric Jones, Robert Kern, Eric Larson, C J Carey, Ilhan Polat, Yu Feng, Eric W. Moore, Jake VanderPlas, Denis Laxalde, Josef Perktold, Robert Cimrman, Ian Henriksen, E. A. Quintero, Charles R. Harris, Anne M. Archibald, Antônio H. Ribeiro, Fabian Pedregosa, Paul van Mulbregt, and SciPy 1.0 Contributors. SciPy 1.0: Fundamental Algorithms for Scientific Computing in Python. *Nature Methods*, 17:261–272, 2020.

[28] Gurobi Optimizer Reference Manual, 2024.

## APPENDIX I. MULTI-AGENT COLLISION AVOIDANCE

The radius (or span) of the  $k$ -th Bézier segment  $B_k^i$  of the  $i$ -th agent quantifies that segment's spatial extent (compactness) and is defined as the maximum Euclidean distance between its geometric centroid,  $\text{cent}(B_k^i)$ , and any of its control points:

$$\text{span}(B_k^i) = \max_{0 \leq l \leq n} \|c_{k,l}^i - \text{cent}(B_k^i)\|_2 \quad (\text{I.1})$$

where  $\text{cent}(B_k^i) = \frac{1}{n+1} \sum_{l=0}^n c_{k,l}^i$ . From constraints (63), it is proved in [26] that, for  $\forall l \in \{1, 2, \dots, n\}$ ,

$$\min \left\{ \|c_{k,l}^i - c_{k,0}^i\|_2, \|c_{k,l}^i - c_{k,n}^i\|_2 \right\} \leq \epsilon_k^i, \quad (\text{I.2})$$

which illustrates that every control point  $c_{k,l}^i$  is close to at least one of the endpoints  $c_{k,0}^i$  or  $c_{k,n}^i$ . Denote  $m_k^* = (c_{k,0}^i + c_{k,n}^i)/2$  as the midpoint of the segment connecting the endpoints. Without loss of generality, assume that  $c_{k,l}^i$  is closer to  $c_{k,0}^i$  than to  $c_{k,n}^i$ . Then,

$$\begin{aligned} \|c_{k,l}^i - m_k^*\|_2 &\leq \|c_{k,l}^i - c_{k,0}^i\|_2 + \|c_{k,0}^i - m_k^*\|_2 \\ &= \epsilon_k^i + \frac{1}{2} \|c_{k,0}^i - c_{k,n}^i\|_2. \end{aligned} \quad (\text{I.3})$$

The same holds if closer to  $c_{k,n}^i$ . Therefore,

$$\begin{aligned} \|\text{cent}(B_k^i) - m_k^*\|_2 &= \left\| \frac{1}{n+1} \sum_{l=0}^n c_{k,l}^i - m_k^* \right\|_2 \\ &\leq \epsilon_k^i + \frac{1}{2} \|c_{k,0}^i - c_{k,n}^i\|_2 \end{aligned} \quad (\text{I.4})$$

Thus, for any control point  $c_{k,l}^i$ ,

$$\begin{aligned} \|c_{k,l}^i - \text{cent}(B_k^i)\|_2 &\leq \|c_{k,l}^i - m_k^*\|_2 + \|\text{cent}(B_k^i) - m_k^*\|_2 \\ &\leq 2\epsilon_k^i + \|c_{k,0}^i - c_{k,n}^i\|_2. \end{aligned} \quad (\text{I.5})$$

yielding  $\text{span}(B_k^i) \leq 2\epsilon_k^i + \|c_{k,0}^i - c_{k,n}^i\|_2$ . since any point at the Bézier curve  $B_k^i(t)$  is within the convex hull,  $\|B_k^i(t) - \text{cent}(B_k^i)\|_2 \leq \text{span}(B_k^i)$ .

Consider any two Bézier curves  $B_k^i$  and  $B_k^j$  over  $t \in [t_k, t_{k+1}]$ , with convex hulls  $\mathcal{CH}_k^i = \{c_{k,l}^i\}_{l=0}^n$  and  $\mathcal{CH}_k^j = \{c_{k,l}^j\}_{l=0}^n$ . The constraint (70) implies that

$$\begin{aligned} \|\text{cent}(B_k^i) - \text{cent}(B_k^j)\|_1 &\geq 2\epsilon_k^i + \|c_{k,0}^i - c_{k,n}^i\|_1 + 2\epsilon_k^j \\ &\quad + \|c_{k,0}^j - c_{k,n}^j\|_1 + \epsilon_{inter}\sqrt{d} \\ &\geq \text{span}(B_k^i) + \text{span}(B_k^j) + (\epsilon_{inter}\sqrt{d}). \end{aligned} \quad (\text{I.6})$$

Then, by the triangle inequality, for any  $t \in [t_k, t_{k+1}]$ ,

$$\begin{aligned} \|B_k^i(t) - B_k^j(t)\|_1 &\geq \|\text{cent}(B_k^i) - \text{cent}(B_k^j)\|_1 \\ &\quad - \text{span}(B_k^i) - \text{span}(B_k^j) \\ &\geq \epsilon_{inter}\sqrt{d}. \end{aligned} \quad (\text{I.7})$$

By the norm inequality  $\|x\|_1 \leq \sqrt{d}\|x\|_2$ , it follows that,

$$\|B_k^i(t) - B_k^j(t)\|_2 \geq \epsilon_{inter}. \quad (\text{I.8})$$

## APPENDIX II. ROTATION MATRIX

This appendix will illustrate how to determine the desired rotation matrix  $R_d(t) = [b_{d,1}(t), b_{d,2}(t), b_{d,3}(t)] \in \text{SO}(3)$ . For ease of notation,  $(t)$  is omitted in the following illustration. Since  $R_d \in \text{SO}(3)$ ,  $b_{d,1}, b_{d,2}, b_{d,3}$  forms an orthonormal basis in  $\mathbb{R}^3$ . This means that  $b_{d,1}, b_{d,2}$  and  $b_{d,3}$  satisfy the following properties:

$$b_{d,1}^\top b_{d,1} = b_{d,2}^\top b_{d,2} = b_{d,3}^\top b_{d,3} = 1, \quad (\text{II.1})$$

$$b_{d,1}^\top b_{d,2} = b_{d,1}^\top b_{d,3} = b_{d,2}^\top b_{d,3} = 0. \quad (\text{II.2})$$

To enhance clarity,  $b_{i,j}$  is used to denote the  $j$ -th element of  $b_{d,i}$ . Firstly, given  $F_d$  in (12), choose  $b_{d,3} = \frac{F_d}{\|F_d\|}$ , specifically,

$$b_{d,3} = \begin{bmatrix} b_{3,1} \\ b_{3,2} \\ b_{3,3} \end{bmatrix} = \frac{1}{\|F_d\|} \begin{bmatrix} F_{d,1} \\ F_{d,2} \\ F_{d,3} \end{bmatrix}. \quad (\text{II.3})$$

The vector  $b_{d,1}$  is then computed from a given  $b_{d,3}$ . Specifically,  $b_{1,3} = -\frac{F_{d,1}}{\|F_d\|}$  is selected, yielding

$$\begin{aligned} b_{d,1}^\top b_{d,3} &= 0 \\ \Rightarrow b_{1,1} \frac{F_{d,1}}{\|F_d\|} + b_{1,2} \frac{F_{d,2}}{\|F_d\|} - \frac{F_{d,1}}{\|F_d\|} \cdot \frac{F_{d,3}}{\|F_d\|} &= 0. \end{aligned} \quad (\text{II.4})$$

Intuitively, choose

$$b_{1,1} = \frac{F_{d,3} + F_{d,2}}{\|F_d\|}, b_{1,2} = -\frac{F_{d,1}}{\|F_d\|}. \quad (\text{II.5})$$

However, without renormalisation one would obtain  $b_{1,2} = b_{1,1}$  and  $\|b_{d,1}\| \neq 1$ . Thus, a scalar  $l > 0$  is introduced to rescale  $b_{1,1}$  and  $b_{1,2}$  for enforcing  $\|b_{d,1}\| = 1$ , namely,

$$b_{1,1} = \frac{F_{d,3} + F_{d,2}l}{\|F_d\|}, b_{1,2} = -\frac{F_{d,1}l}{\|F_d\|},$$

$$\text{and } b_{1,1}^2 + b_{1,2}^2 + b_{1,3}^2 = 1,$$

$$\Rightarrow b_{1,1}^2 + b_{1,2}^2 = 1 - \frac{F_{d,1}^2}{\|F_d\|^2} = \frac{F_{d,2}^2 + F_{d,3}^2}{\|F_d\|^2}, \quad (\text{II.6})$$

$$\Rightarrow (F_{d,3} + F_{d,2}l)^2 + (F_{d,1}l)^2 = F_{d,2}^2 + F_{d,3}^2,$$

$$\Rightarrow (\|F_d\|^2 - F_{d,3}^2)l^2 + 2F_{d,3}F_{d,2}l - F_{d,2}^2 = 0,$$

$$\Rightarrow l = \frac{F_{d,2}}{\|F_d\| + F_{d,3}}.$$

Therefore, the following is obtained.

$$b_{d,1} = \begin{bmatrix} b_{1,1} \\ b_{1,2} \\ b_{1,3} \end{bmatrix} = \frac{1}{\|F_d\|} \begin{bmatrix} F_{d,3} + \frac{F_{d,2}^2}{\|F_d\| + F_{d,3}} \\ -\frac{F_{d,1}F_{d,2}}{\|F_d\| + F_{d,3}} \\ -F_{d,1} \end{bmatrix}. \quad (\text{II.7})$$

The orthogonality condition  $b_{d,1}^\top b_{d,3} = 0$  can be verified to hold. Subsequently, solving  $b_{d,2} = b_{d,3} \times b_{d,1}$  yields

$$b_{d,2} = \begin{bmatrix} b_{2,1} \\ b_{2,2} \\ b_{2,3} \end{bmatrix} = \frac{1}{\|F_d\|} \begin{bmatrix} -\frac{F_{d,1}F_{d,2}}{\|F_d\| + F_{d,3}} \\ F_{d,3} + \frac{F_{d,1}^2}{\|F_d\| + F_{d,3}} \\ -F_{d,2} \end{bmatrix}.$$

### APPENDIX III. PROOF OF LYAPUNOV BOUNDS

For  $t \in \mathbb{T}$ , the derivatives of the error functions  $e_p(t)$ ,  $e_v(t)$ ,  $\Psi_K(t)$ ,  $e_{K,R}(t)$ , and  $e_\omega(t)$  in (6)-(10) are obtained by (See Appendix VI)

$$\dot{e}_p(t) = e_v(t), \quad (\text{III.1})$$

$$\dot{e}_v(t) = -\frac{1}{m}(K_p e_p(t) + K_v e_v(t) + \Delta_f(t)), \quad (\text{III.2})$$

$$\dot{\Psi}_K(t) = e_{K,R}^\top(t) e_\omega(t), \quad (\text{III.3})$$

$$\dot{e}_{K,R}(t) = \mathcal{C}(t) e_\omega(t), \quad (\text{III.4})$$

$$\dot{e}_\omega(t) = -J^{-1}(e_{K,R}(t) + K_\omega e_\omega(t)), \quad (\text{III.5})$$

where

$$\mathcal{C}(t) := \frac{1}{2}(\text{tr}[K_R R_d(t) R(t)] I_3 - K_R R_d(t) R(t)), \quad (\text{III.6})$$

$$\Delta_f(t) := \|F_d(t)\|((b_{3,d}(t) - b_{3,d}^\top(t) b_3(t)) b_3(t)). \quad (\text{III.7})$$

*Lemma 1* ([20, Proposition 2]): Let  $t \in \mathbb{T}$ , then  $\|\mathcal{C}(t)\|_2 \leq \frac{1}{\sqrt{2}} \text{tr}[K_R]$ .

*Lemma 2* (See Appendix V): Given  $t \in \mathbb{T}$ , suppose  $K_R = \text{diag}(k_{R_1}, k_{R_2}, k_{R_3})$  is a diagonal positive-definite matrix,  $R(t), R_d(t) \in \text{SO}(3)$ , and  $\Psi_K(t) < \psi$  for some constant  $\psi \in (0, h_1)$ . Define  $b_3(t)$  and  $b_{3,d}(t)$  as the third columns of  $R(t)$  and  $R_d(t)$ , respectively. Then:

$$\|(b_{3,d}(t) - b_{3,d}^\top(t) b_3(t)) b_3(t)\| \leq \sqrt{\frac{4g_2}{h_1}} \|e_{K,R}\|. \quad (\text{III.8})$$

This further implies that

$$\|\Delta_f(t)\| \leq (\| [K_p \ K_v] M_1^{-\frac{1}{2}} \| \sqrt{\mathcal{V}_1(t)} + m \|b_a\|) \sqrt{\frac{4g_2}{h_1}} \|e_{K,R}\|. \quad (\text{III.9})$$

Since  $\|\mathcal{C}(t)\| \leq \frac{1}{\sqrt{2}} \text{tr}[K_R]$  in Lemma 1, the time derivative of  $\mathcal{V}_2(t)$  is bounded by

$$\begin{aligned} \dot{\mathcal{V}}_2(t) &= e_{K,R}^\top(t) (c_2 J^{-1}) e_{K,R}(t) - e_\omega^\top(t) c_2 K_w J^{-1} e_{K,R}(t) \\ &\quad - e_\omega^\top(t) (K_w - c_2 \mathcal{C}(t)) e_\omega(t) \\ &\leq -e_{K,R}^\top(t) (c_2 J^{-1}) e_{K,R}(t) - e_\omega^\top(t) c_2 K_w J^{-1} e_{K,R}(t) \\ &\quad - e_\omega^\top(t) \left( K_w - \frac{c_2}{\sqrt{2}} \text{tr}[K_R] I_3 \right) e_\omega(t) \\ &= z_2^\top(t) W_2 z_2(t). \end{aligned} \quad (\text{III.10})$$

With the generalized Rayleigh inequality, there exists

$$\begin{aligned} \dot{\mathcal{V}}_2(t) &\leq -\|W_2^{\frac{1}{2}} z_2(t)\|^2 \\ &\leq -\lambda \left( M_{2,2}^{-\frac{1}{2}} W_2 M_{2,2}^{-\frac{1}{2}} \right) \left\| M_{2,2}^{\frac{1}{2}} z_2 \right\|^2 \\ &\leq -\lambda \left( M_{2,2}^{-\frac{1}{2}} W_2 M_{2,2}^{-\frac{1}{2}} \right) \mathcal{V}_2(t). \end{aligned} \quad (\text{III.11})$$

By Grönwall's inequality, it follows that

$$\mathcal{V}_2(t) \leq e^{-\beta t} \mathcal{V}_2(0), \quad (\text{III.12})$$

where  $\beta = \lambda \left( M_{2,2}^{-\frac{1}{2}} W_2 M_{2,2}^{-\frac{1}{2}} \right)$ . This implies

$$\sqrt{\mathcal{V}_2(t)} \leq e^{-\frac{\beta}{2} t} \sqrt{\mathcal{V}_2(0)}. \quad (\text{III.13})$$

Since  $z_2^\top(t) M_{2,1} z_2(t) \leq \mathcal{V}_2(t) \leq e^{-\beta t} \mathcal{V}_2(0)$ , implying that

$$\begin{aligned} \|e_{K,R}(t)\| &\leq \left\| [I_3, 0_3] M_{2,1}^{-\frac{1}{2}} \right\| \sqrt{\mathcal{V}_2(t)} \\ &\leq \left\| [I_3, 0_3] M_{2,1}^{-\frac{1}{2}} \right\| e^{-\frac{\beta}{2} t} \sqrt{\mathcal{V}_2(0)}. \end{aligned} \quad (\text{III.14})$$

Define

$$\alpha_0 = \lambda \left( M_1^{-\frac{1}{2}} W_1 M_1^{-\frac{1}{2}} \right), \quad (\text{III.15})$$

$$\alpha_1 = \left\| \left[ \frac{c_1}{m} I_3, I_3 \right] M_1^{-\frac{1}{2}} \right\| \left\| [K_p, K_v] M_1^{-\frac{1}{2}} \right\| \beta', \quad (\text{III.16})$$

$$\alpha_2 = m \|b_a\| \left\| \left[ \frac{c_1}{m} I_3, I_3 \right] M_1^{-\frac{1}{2}} \right\| \beta', \quad (\text{III.17})$$

$$\beta' = \left\| [I_3, 0_{3 \times 3}] M_{2,1}^{-\frac{1}{2}} \right\| \sqrt{\frac{4g_2}{h_1}}. \quad (\text{III.18})$$

With Lemma 2, (III.1) and (III.2), the time derivative of  $\mathcal{V}_1(t)$  is bounded by

$$\begin{aligned} \dot{\mathcal{V}}_1(t) &= -\frac{c_1}{m} e_p^\top(t) K_p e_p(t) - \frac{c_1}{m} e_p^\top(t) K_v e_v(t) \\ &\quad - e_v^\top(t) (K_v - c_1 I_3) e_v(t) - \Delta_f^\top \left( \frac{c_1}{m} e_p(t) + e_v(t) \right) \\ &= -z_1^\top(t) W_1 z_1(t) - \Delta_f^\top(t) \left[ \frac{c_1}{m} I_3 \ I_3 \right] z_1(t) \\ &\leq -\lambda (M_1^{-\frac{1}{2}} W_1 M_1^{-\frac{1}{2}}) \mathcal{V}_1(t) + \|\Delta_f(t)\| \left\| \left[ \frac{c_1}{m} I_3 \ I_3 \right] z_1(t) \right\| \\ &\leq -(\alpha_0 - \alpha_1 \sqrt{\mathcal{V}_2(t)}) \mathcal{V}_1(t) + \alpha_2 \sqrt{\mathcal{V}_2(t)} \mathcal{V}_1(t) \\ &\leq -(\alpha_0 - \alpha_1 e^{-\frac{\beta}{2} t} \sqrt{\mathcal{V}_2(0)}) \mathcal{V}_1(t) \\ &\quad + \alpha_2 e^{-\frac{\beta}{2} t} \sqrt{\mathcal{V}_2(0)} \sqrt{\mathcal{V}_1(t)}. \end{aligned} \quad (\text{III.19})$$

Since  $\sqrt{\mathcal{V}_2(t)} \leq \mathcal{L}_2(\mathcal{V}_2(0), t)$ , using a nonlinear Grönwall-type inequality for (37) yields  $\sqrt{\mathcal{V}_1(t)} \leq \mathcal{L}_1(\mathcal{V}_1(0), \mathcal{V}_2(0), t)$  where

$$\begin{aligned} \mathcal{L}_1(\mathcal{V}_1(0), \mathcal{V}_2(0), t) &= e^{-\frac{\alpha_0 t}{2}} \left[ e^{\frac{\alpha_1 \sqrt{\mathcal{V}_2(0)}}{\beta}} \sqrt{\mathcal{V}_1(0)} \right. \\ &\quad \left. + \frac{\alpha_2 \sqrt{\mathcal{V}_2(0)}}{2} \int_0^t e^{\frac{1}{2}(\alpha_0 - \beta)s} ds \right]. \end{aligned} \quad (\text{III.20})$$

### APPENDIX IV. PROOF OF INITIAL CONDITIONS

With  $g_1 \|e_{K,R}(t)\|^2 \leq \Psi_K(t)$  in Proposition 1, if the initial condition  $\frac{1}{2} e_\omega^\top(0) J e_\omega(0) \leq (1 - \alpha_\psi) \psi$  and  $\Psi(0) \leq \alpha_\psi \psi$  are satisfied, then,

$$\begin{aligned} \mathcal{V}_2(0) &= \frac{1}{2} e_\omega^\top(0) J e_\omega(0) + \Psi_K(0) + c_2 e_R^\top(0) e_\omega(0) \\ &\leq (1 - \alpha_\psi) \psi + \alpha_\psi \psi + c_2 \|e_{K,R}(0)\| \|e_\omega(0)\| \\ &\leq \psi + c_2 \sqrt{\frac{\psi}{g_1}} \|J^{-1/2}\| \|J^{1/2} e_\omega(0)\| \\ &\leq \psi + c_2 \sqrt{\frac{\psi}{g_1}} \|J^{-1/2}\| \sqrt{2(1 - \alpha_\psi) \psi} \\ &= \left( 1 + c_2 \sqrt{\frac{2(1 - \alpha_\psi)}{\lambda(J) g_1}} \right) \psi = \bar{\mathcal{V}}_2. \end{aligned}$$

Given  $z_1(t) = [e_p(t), e_v(t)]^\top$ ,

$$\begin{aligned} e_p(t) &= [I_3, 0_{3 \times 3}] z_1(t) = [I_3, 0_{3 \times 3}] M_1^{-\frac{1}{2}} M_1^{\frac{1}{2}} z_1(t) \\ \Rightarrow \|e_p(t)\| &\leq \|[I_3, 0_{3 \times 3}] M_1^{-\frac{1}{2}}\| \|M_1^{\frac{1}{2}} z_1(t)\| \end{aligned}$$

Since  $\mathcal{V}_1(t) = (M_1^{\frac{1}{2}} z_1(t))^\top (M_1^{\frac{1}{2}} z_1(t)) = \|M_1^{\frac{1}{2}} z_1(t)\|^2 \Rightarrow \sqrt{\mathcal{V}_1(t)} = \|M_1^{\frac{1}{2}} z_1(t)\|$ . Since the function  $\mathcal{L}(\mathcal{V}_1(0), \mathcal{V}_2(0), t)$  is non-decreasing with respect to  $\mathcal{V}_1(0)$  and  $\mathcal{V}_2(0)$ , it follows that  $\sqrt{\mathcal{V}(t)} \leq \mathcal{L}(\bar{\mathcal{V}}_1, \bar{\mathcal{V}}_2, t)$ . Therefore,

$$\begin{aligned} \|e_p(t)\| &\leq \|[I_3, 0_{3 \times 3}] M_1^{-\frac{1}{2}}\| \sqrt{\mathcal{V}_1(t)} \\ &\leq \|[I_3, 0_{3 \times 3}] M_1^{-\frac{1}{2}}\| \mathcal{L}_1(\bar{\mathcal{V}}_1, \bar{\mathcal{V}}_2, t) \\ &= \mathcal{L}_p(\bar{\mathcal{V}}_1, \bar{\mathcal{V}}_2, t) \end{aligned}$$

Likewise, the other error bounds can be derived as

$$\begin{aligned} \|e_v(t)\| &= \|[0_{3 \times 3}, I_3] M_1^{-\frac{1}{2}} M_1^{\frac{1}{2}} z_1(t)\| \\ &\leq \|[0_{3 \times 3}, I_3] M_1^{-\frac{1}{2}}\| \mathcal{L}_1(\bar{\mathcal{V}}_1, \bar{\mathcal{V}}_2, t) \end{aligned}$$

#### APPENDIX V. PROOF OF LEMMA 2

*Proof:* Let  $G(t) := R_d^\top(t)R(t) \in \text{SO}(3)$ , then it can be rewritten as

$$\begin{aligned} \|(b_{3,d}(t) - b_{3,d}^\top(t)b_3(t)) b_3(t)\|^2 &= 1 - ((b_{3,d}(t) \cdot b_3(t)))^2 \\ &= 1 - (G_{3,3}(t))^2. \end{aligned} \quad (\text{V.1})$$

where  $G_{3,3}(t)$  is the element in the third row and third column of the matrix  $G(t)$ .

Let  $x = [x_1, x_2, x_3]^\top \in \mathbb{R}^3$  be the rotation vector such that  $G(t) = \exp(\hat{x})$ , where  $\hat{x} \in \mathfrak{so}(3)$  is the skew-symmetric matrix associated with  $x$  and the rotation angle is  $\|x\| = \theta \in [0, \pi]$ . Define the unit rotation axis  $u = x/\|x\| = [u_1, u_2, u_3]^\top$ . By Rodrigues' rotation formula,

$$G(t) = I + \sin \theta \hat{u} + (1 - \cos \theta) \hat{u}^2. \quad (\text{V.2})$$

Using the standard component form of Rodrigues' formula, the (3, 3) element of  $G(t)$  is given by

$$\begin{aligned} G_{3,3}(t) &= \cos \theta + (1 - \cos \theta) u_3^2 \\ &= \cos \theta + (1 - \cos \theta) \frac{x_3^2}{\|x\|^2}. \end{aligned} \quad (\text{V.3})$$

Define

$$T := \frac{(x_1^2 + x_2^2)(\cos \theta - 1)}{\|x\|^2}, \quad (\text{V.4})$$

then (V.3) implies  $G_{3,3} = 1 + T$ , thus,

$$1 - G_{3,3}^2 = 1 - (1 + T)^2 = -2T - T^2 \leq -2T. \quad (\text{V.5})$$

Because  $(x_1^2 + x_2^2)/\|x\|^2 \leq 1$  and  $1 - \cos \theta \geq 0$ ,

$$\begin{aligned} 1 - G_{3,3}^2 &\leq -2T \\ &= 2 \frac{(x_1^2 + x_2^2)(1 - \cos \theta)}{\|x\|^2} \\ &\leq 2(1 - \cos \theta). \end{aligned} \quad (\text{V.6})$$

From [20],  $\Psi_K$  can be expressed as

$$\Psi_K = \frac{1 - \cos(\|x\|)}{2\|x\|^2} \sum_{(i,j,k) \in \mathcal{C}} (k_{R,i} + k_{R,j}) x_k^2. \quad (\text{V.7})$$

where  $\mathcal{C} = \{(1, 2, 3), (2, 3, 1), (3, 1, 2)\}$ .

Since  $h_1 = \min \{k_{R_1} + k_{R_2}, k_{R_2} + k_{R_3}, k_{R_1} + k_{R_3}\}$ ,

$$\sum_{(i,j,k) \in \mathcal{C}} (k_{R,i} + k_{R,j}) x_k^2 \geq h_1 \sum_{k=1}^3 x_k^2 = h_1 \|x\|^2. \quad (\text{V.8})$$

Putting it back into (V.7) leads to

$$\begin{aligned} \Psi_K &\geq \frac{1 - \cos(\|x\|)}{2\|x\|^2} (h_1 \|x\|^2) \\ &= \frac{h_1}{2} (1 - \cos(\|x\|)). \end{aligned} \quad (\text{V.9})$$

This implies that  $1 - \cos(\|x\|) \leq \frac{2}{h_1} \Psi$ , which yields

$$\begin{aligned} \|(b_{3,d}(t) - b_{3,d}^\top(t)b_3(t)) b_3(t)\|^2 &= 1 - G_{3,3}^2 \\ &\leq 2(1 - \cos(\|x\|)) \\ &\leq \frac{4}{h_1} \Psi. \end{aligned} \quad (\text{V.10})$$

Using the quadratic bounds  $\Psi_K(t) \leq g_2 \|e_{K,R}\|^2(t)$ ,

$$\|(b_{3,d}(t) - b_{3,d}^\top(t)b_3(t)) b_3(t)\| \leq \sqrt{\frac{4g_2}{h_1}} \|e_{K,R}\|. \quad (\text{V.11})$$

Combining with the definition of  $F_d(t)$  in (12) and Assumption 1, using the triangular inequality gives

$$\begin{aligned} \|F_d(t)\| &\leq \|-K_p e_p(t) - K_v e_v(t) + m g e_3 + m \ddot{y}_d(t)\| \\ &\leq \|K_p e_p(t) + K_v e_v(t)\| + m \|b_a\| \end{aligned} \quad (\text{V.12})$$

Furthermore, using the definitions of  $\mathcal{V}_1(t)$  in (22) yields

$$\begin{aligned} \|K_p e_p(t) + K_v e_v(t)\| &= \|[K_p \ K_v] z_1(t)\| \\ &\leq \|[K_p \ K_v] M_1^{-\frac{1}{2}}\| \sqrt{\mathcal{V}_1(t)} \end{aligned} \quad (\text{V.13})$$

Therefore,  $\|\Delta_f(t)\|$  is bounded by:

$$\begin{aligned} \|\Delta_f(t)\| &\leq \|F_d(t)\| \|(b_{3,d}(t) - b_{3,d}^\top(t)b_3(t)) b_3(t)\| \\ &\leq (\|[K_p \ K_v] M_1^{-\frac{1}{2}}\| \sqrt{\mathcal{V}_1(t)} \\ &\quad + m \|b_a\|) \sqrt{\frac{4g_2}{h_1}} \|e_{K,R}\|. \end{aligned}$$

Since  $z_2^\top(t) M_{2,1} z_2(t) \leq \mathcal{V}_2(t)$ , then,

$$\|e_{K,R}(t)\| \leq \|[I_3, 0_{3 \times 3}] M_{2,1}^{-\frac{1}{2}}\| \sqrt{\mathcal{V}_2(t)}. \quad (\text{V.14})$$

#### APPENDIX VI. DERIVATIVES OF THE ERROR FUNCTIONS

This appendix shows how to calculate the derivative of these error functions.

• **The derivative of  $e_p(t)$ :**

$$\dot{e}_p(t) = \dot{y}_{tr}(t) - \dot{y}_d(t) = e_v(t).$$

• **The derivative of  $e_v(t)$ :**

From (3) and (21) in Assumption 1, it follows that

$$m \dot{y}_{tr}(t) = -m g e_3 + f(t) R(t) e_3, \quad (\text{VI.1})$$

$$m \dot{y}_d(t) = F_d(t) + K_p e_p(t) + K_v e_v(t) - m g e_3. \quad (\text{VI.2})$$

Therefore,

$$\begin{aligned}
m\dot{e}_v(t) &= m\ddot{y}_{tr}(t) - m\ddot{y}_d(t) \\
&= (-mge_3 + f(t)R(t)e_3) \\
&\quad - (F_d(t) + K_p e_p(t) + K_v e_v(t) - mge_3) \\
&= -(K_p e_p(t) + K_v e_v(t)) - (F_d(t) - f(t)R(t)e_3).
\end{aligned} \tag{VI.3}$$

Since  $f(t) = F_d^\top(t)R(t)e_3$  and  $b_{3,d}(t) = \frac{F_d(t)}{\|F_d(t)\|}$ , then,

$$\begin{aligned}
F_d^\top(t)R(t)e_3 &= F_d^\top(t)b_3(t) \\
&= \|F_d(t)\| \frac{F_d^\top(t)}{\|F_d(t)\|} b_3(t) \\
&= \|F_d(t)\| (b_{3,d}^\top(t)b_3(t)).
\end{aligned} \tag{VI.4}$$

Thus,

$$\begin{aligned}
F_d(t) - f(t)R(t)e_3 &= \|F_d(t)\| \frac{F_d(t)}{\|F_d(t)\|} - (F_d^\top(t)R(t)e_3)R(t)e_3 \\
&= \|F_d(t)\| b_3(t) - \|F_d(t)\| (b_{3,d}^\top(t)b_3(t)) b_3(t) \\
&= \|F_d(t)\| ((b_{3,d}(t) - b_{3,d}^\top(t)b_3(t)) b_3(t)) \\
&\triangleq \Delta_f(t). \\
\Rightarrow \dot{e}_v(t) &= -\frac{1}{m}(K_p e_p(t) + K_v e_v(t) + \Delta_f(t)).
\end{aligned} \tag{VI.5}$$

• **The derivative of  $\Psi_K(t)$ :**

Let  $G(t) = R_d^\top(t)R(t) \in \text{SO}(3)$ , then

$$\dot{\Psi}_K(t) = \frac{1}{2} \text{tr}(-K_R \dot{G}(t)). \tag{VI.6}$$

Moreover, with  $\hat{\omega}_d(t) \in \mathfrak{so}(3)$ , the following properties hold:

$$\hat{\omega}_d^\top(t) = -\hat{\omega}_d(t) \tag{VI.7}$$

$$G(t)G^\top(t) = 1 \tag{VI.8}$$

$$G^\top(t)\hat{\omega}_d(t)G(t) = (G^\top(t)\omega_d(t))^\wedge. \tag{VI.9}$$

Using these identities, the derivative of  $G(t)$  can be computed as

$$\begin{aligned}
\dot{G}(t) &= \dot{R}_d^\top(t)R(t) + R_d^\top(t)\dot{R}(t) \\
&= (R_d(t)\hat{\omega}_d(t))^\top R(t) + G(t)\hat{\omega}(t) \\
&= -\hat{\omega}_d(t)G(t) + G(t)\hat{\omega}(t) \\
&= G(t)(\hat{\omega}(t) - G^\top(t)\hat{\omega}_d(t)G(t)) \\
&= G(t)\left(\hat{\omega}(t) - (G^\top(t)\omega_d(t))^\wedge\right) \\
&= G(t)(\omega(t) - G^\top(t)\omega_d(t))^\wedge \\
&= G(t)\hat{e}_\omega(t).
\end{aligned} \tag{VI.10}$$

Using the trace identity  $\text{tr}[A\hat{x}] = -x^\top(A - A^\top)^\vee$  and the definition of  $e_{K,R}(t)$  yields

$$\begin{aligned}
\dot{\Psi}(t) &= -\frac{1}{2} \text{tr}(K_R G(t)\hat{e}_\omega(t)) \\
&= \frac{1}{2} e_\omega^\top(t) (K_R G(t) - (K_R G(t))^\top)^\vee \\
&= e_\omega^\top(t) e_{K,R}(t).
\end{aligned} \tag{VI.11}$$

• **The derivative of  $e_{K,R}(t)$ :**

$$\begin{aligned}
\dot{e}_{K,R}(t) &= \frac{1}{2} \left( K_R \dot{G}(t) - \dot{G}^\top(t)K_R \right)^\vee \\
&= \frac{1}{2} \left( K_R G(t)\hat{e}_\omega(t) + \hat{e}_\omega(t)G^\top(t)K_R \right)^\vee.
\end{aligned} \tag{VI.12}$$

Since  $A\hat{x} + \hat{x}A^\top = ((\text{tr}(A)I - A)x)^\wedge$ , let  $A(t) = K_R G(t)$ , since  $K_R$  is a diagonal matrix,  $A(t)^\top = G^\top(t)K_R$ . Hence,

$$\begin{aligned}
\dot{e}_{K,R}(t) &= \frac{1}{2} \left( A(t)\hat{e}_\omega(t) + \hat{e}_\omega(t)A^\top(t) \right)^\vee \\
&= \frac{1}{2} (\text{tr}(A(t))I_3 - A(t)) e_\omega(t) \\
&= \mathcal{C}(t)e_\omega(t).
\end{aligned} \tag{VI.13}$$

where  $\mathcal{C}(t) := \frac{1}{2} (\text{tr}(K_R R_d^\top(t)R(t))I_3 - K_R R_d^\top(t)R(t))$ .

• **The derivative of  $e_\omega(t)$ :**

Rewrite  $e_\omega(t) = \omega(t) - G^\top(t)\omega_d(t)$ , then

$$\begin{aligned}
\dot{e}_\omega(t) &= \dot{\omega}(t) - \dot{G}^\top(t)\omega_d(t) - G^\top(t)\dot{\omega}_d(t) \\
&= \dot{\omega}(t) - \hat{e}_\omega^\top(t)G^\top(t)\omega_d(t) - G^\top(t)\dot{\omega}_d(t).
\end{aligned} \tag{VI.14}$$

Given the definition of  $\dot{\omega}(t)$  and  $\tau(t)$ , it follows that

$$\begin{aligned}
\dot{e}_\omega(t) &= J^{-1}(-\omega(t) \times J\omega(t) + \tau(t)) \\
&\quad + \hat{e}_\omega(t)G^\top(t)\omega_d(t) - G^\top(t)\dot{\omega}_d(t) \\
&= J^{-1}(-e_{K,R}(t) - k_\omega e_\omega(t)) \\
&\quad - \hat{\omega}(t)G^\top(t)\omega_d(t) + \hat{e}_\omega(t)G^\top(t)\omega_d(t)
\end{aligned} \tag{VI.15}$$

With the property of hat operator  $R\hat{x}R^\top = (Rx)^\wedge$ , it follows that

$$\begin{aligned}
\hat{e}_\omega(t) &= (\omega(t) - G^\top(t)\omega_d(t))^\wedge \\
&= \hat{\omega}(t) - (G^\top(t)\omega_d(t))^\wedge \\
&= \hat{\omega}(t) - G^\top(t)\hat{\omega}_d(t)G(t).
\end{aligned} \tag{VI.16}$$

Since  $G(t)G^\top(t) = 1$  and  $\hat{\omega}_d(t)\omega_d(t) = 0$ , then,

$$\begin{aligned}
\hat{e}_\omega(t)G^\top(t)\omega_d(t) - \hat{\omega}(t)G^\top(t)\omega_d(t) &= 0 \\
\Rightarrow \dot{e}_\omega(t) &= -J^{-1}(e_{K,R}(t) + k_\omega e_\omega(t)).
\end{aligned} \tag{VI.17}$$